Research Square

Preprints are preliminary reports that have not undergone peer review.
They should not be considered conclusive, used to inform clinical practice,
or referenced by the media as validated information.

Lenticulostriate arteries supplying the pyramidal tract: Anatomy and intraoperative landmarks for preservation during resection of adjacent gliomas

Yuto Shingai
Tohoku University Graduate School of Medicine
Masayuki Kanamori
masayuki.kanamori.e8@tohoku.ac.jp
Tohoku University Graduate School of Medicine
Shin-Ichiro Osawa
Tohoku University Graduate School of Medicine
Yoshiteru Shimoda
Tohoku University Graduate School of Medicine
Kazuki Shimada
Tohoku University Hospital, Tohoku University
Kazutoshi Shirotori
Tohoku University Hospital, Tohoku University
Shingo Kayano
Tohoku University Hospital, Tohoku University
Yoshinari Osada
Tohoku University Graduate School of Medicine
Shota Yamashita
Tohoku University Graduate School of Medicine
Shunji Mugikura
Tohoku University Graduate School of Medicine
Hidenori Endo
Tohoku University Graduate School of Medicine

Research Article

Keywords: Ultra-high-resolution computed tomography, Computed tomography angiography, Lenticulostriate artery, Pyramidal tract, Glioma

Posted Date: October 27th, 2026

DOI: https://doi.org/10.21203/rs.3.rs-11116044/v1

License: This work is licensed under a Creative Commons Attribution 4.0 International License.
Read Full License

Additional Declarations: No competing interests reported.

Abstract

Purpose

This study characterized the anatomical course of the lenticulostriate arteries supplying the pyramidal tract (PT-LSAs) and identified intraoperative landmarks for their preservation.

Methods

The course of PT-LSAs was evaluated in 10 patients with glioma or epilepsy without LSA displacement. Analysis integrated ultrahigh-resolution intra-arterial computed tomography angiography (UHR-IA-CTA) with multiple imaging modalities.

Results

The PT-LSAs were located in the posterolateral LSA territory and supplied the PT along the posteromedial putamen. Based on their relationship with the insular central sulcus (ICS), PT-LSA stems were classified as anterior or posterior PT-LSAs. The anterior PT-LSAs coursed cranially and supplied the anterolateral and superior PT adjacent to the putamen in six cases. The posterior PT-LSAs coursed posteriorly and cranially and supplied the posteromedial and inferior PT adjacent to the putamen in nine cases. The anterior and posterior PT-LSAs coursed along the putamen surface in five and four cases, respectively. Both types changed direction medially and cranially, defining the region most vulnerable to injury during insular and temporal glioma resection. The anterior PT-LSA curve was located beneath the ICS and anterior long gyri (ALG), whereas the posterior PT-LSA curve was located beneath the ALG and posterior long gyri and near the anterior end of the choroid plexus. The ICS and choroid plexus were useful intraoperative landmarks for localizing the PT-LSAs during glioma resection in their vicinity.

Conclusion

The anatomical characteristics of the PT-LSAs may facilitate safe resection of gliomas adjacent to the LSAs.

Introduction

The lenticulostriate arteries (LSAs) are clinically important perforating vessels associated with hemorrhagic and ischemic stroke [2, 31, 33]. Injury to these arteries during craniotomy can cause severe motor deficits [11, 12, 16, 22, 30]. To minimize these complications, numerous anatomical studies have examined the course of the LSAs. Previous studies using vascular casts of cerebral hemispheres without neurological disease described their anatomy in detail [6, 7, 19, 20]. The LSAs originate from the distal M1 or proximal M2 segment of the middle cerebral artery (MCA), and their extracerebral portions

course posteromedially toward the anterior perforated substance [6, 19, 20]. After penetrating the anterior perforated substance, the proximal intracerebral segments are arranged rostrocaudally and mediolaterally, forming a fan-shaped distribution. Prominent curves or loops frequently occur at the junction between the proximal and distal intracerebral segments in coronal, sagittal, axial, or oblique planes. The proximal intracerebral LSAs give rise to the longitudinal and transverse branches, whereas the distal intracerebral LSAs give rise to terminal branches. The LSAs typically supply the superior genu of the internal capsule, rostral posterior limb of the internal capsule, putamen, most of the lateral globus pallidus, superior portions of the caudate head and body, external capsule, and anterior commissure [33–35]. Although anastomoses between LSAs may occur within the cistern, none are present within the brain parenchyma [7, 20]. Consequently, injury to an LSA within a tumor or at the deep resection margin inevitably causes ischemia in its corresponding parenchymal territory [10]. These considerations underscore the importance of accurate preoperative assessment and intraoperative preservation of the LSA supplying the pyramidal tract (PT-LSA).

Several methods have been proposed for preoperative evaluation of LSA anatomy, including catheter angiography [22], gadolinium-enhanced three-dimensional (3D) time-of-flight magnetic resonance imaging (MRI) [26], 3D constructive interference in steady-state sequences, multimodal image-based assessments combining MRI and angiography [5], 7.0-Tesla magnetic resonance angiography (MRA) [3, 14], and 3D rotational digital subtraction angiography (3D-DSA) [15]. However, the anatomical course of the PT-LSA and its relationship to adjacent structures remain incompletely characterized because of the limited spatial resolution of these modalities. Recently, ultrahigh-resolution (UHR) computed tomography (CT), equipped with a 0.25-mm detector, was introduced, and UHR intravenous CT angiography (CTA) improved visualization of the LSAs [21]. We previously showed the utility of UHR intra-arterial CTA (UHR-IA-CTA) for visualizing the PT-LSA, long insular arteries, long medullary arteries, and anterior choroidal artery perforators supplying the PT, with superior performance compared with high-resolution 3D-DSA [13, 23, 27]. These high-resolution images enable *in vivo* characterization of LSA anatomy and accurate preoperative assessment of LSA involvement in gliomas extending adjacent to these vessels. Improved anatomical characterization may also facilitate identification of reliable intraoperative landmarks for PT-LSA localization.

In this study, we investigated the anatomical course of the PT-LSAs in patients without signal abnormalities or structural distortion around the LSAs using UHR-IA-CTA. Based on these findings, we identified anatomical landmarks that facilitate preservation of the PT-LSAs during surgery.

Methods

Ethics

This study was conducted in accordance with the Declaration of Helsinki and was approved by the Institutional Review Board of our hospital (2022-1-447). Written informed consent was obtained from all patients.

Patients

From September, 2022 to December, 2024, patients scheduled for resection of a glioma or epileptogenic lesion at risk of PT ischemia have undergone preoperative evaluation of the perforating arteries supplying the PT using UHR-IA-CTA. For analysis of LSA anatomical characteristics, we included 10 patients without abnormal MRI signal intensity or structural distortion involving the LSAs, PT, or basal ganglia (BG). We also examined one patient with an isocitrate dehydrogenase (IDH)-mutant temporal astrocytoma extending into the insula and putamen to assess the utility of anatomical landmarks for intraoperative identification of the PT-LSA.

UHR-IA-CTA Protocol

UHR-IA-CTA was performed as previously described [13, 23, 27]. The protocol consisted of four steps: (1) endovascular procedure, (2) UHR-IA-CTA image acquisition, (3) MRI acquisition, and (4) image post-processing.

1. Endovascular procedure: A 4-French sheath (CX, 115 cm; Gadelius Medical, Tokyo, Japan) was inserted over a 0.035-inch Radifocus guidewire (Terumo, Tokyo, Japan) into the cervical segment of the internal carotid artery (ICA) through the right radial artery. DSA was performed, and the capillary phase and time-to-peak were evaluated. A 4-French catheter was advanced
2. UHR-IA-CTA acquisition: UHR-IA-CTA was performed using a 160-detector-row scanner (Aquilion Precision; Canon Medical Systems, Otawara, Japan) with a 1024 × 1024 matrix and a slice thickness of 0.25 mm. A total of 9 mL of iodinated contrast medium (Omnipaque 350 or Iopamiron 370) was injected at a rate of 3 mL with a delay of 1.5–2.0 seconds.
3. MRI acquisition: To evaluate lesion extent and its anatomical relationship to the BG and PT, 3D T1-weighted imaging (3D-T1WI), gadolinium-enhanced T1WI (3D-Gd-T1WI), and diffusion tensor imaging (DTI) were acquired using a 3.0-T MRI scanner (Intera Achieva 3.0T Quasar Dual; Philips Medical Systems, Best, the Netherlands).
4. Image processing: Image processing was performed using commercially available software (Ziostation2; Ziosoft, Tokyo, Japan) and Brainlab Elements (Brainlab, Munich, Germany).

The PT was reconstructed using DTI–based tractography. Regions of interest were manually placed in the precentral gyrus and cerebral peduncle for fiber tracking. The tracking parameters included a minimum fractional anisotropy threshold of 0.15, a minimum fiber length of 500 mm, and a maximum turning angle of 20°. The reconstructed fiber tracts were independently reviewed and confirmed to represent the PT by a neurosurgeon (MK) and a neuroradiologist (SM).

Using fused UHR-IA-CTA, MR tractography, and three-dimensional T1-weighted imaging (3D-T1WI), in which the putamen and internal and globus pallidus were automatically segmented (Supplementary Fig. 1A), PT-LSAs were identified as vessels directly crossing the PT on the fusion images (yellow and white arrows in Supplementary Fig. 1A).

To assess the anatomical characteristics of the LSAs and PT-LSAs, 3D maximum intensity projection (3D-MIP) images of the LSAs were generated from UHR-IA-CT by manually segmenting the LSA territory to eliminate interference from cortical branches, as previously described [13]. These images were subsequently overlaid with MR tractography of the PT to create fused images of the PT and LSAs, and the corresponding proximal PT-LSA stems were mapped based on their morphological features (Supplementary Fig. 1B).

To predict the PT-LSA course during surgery, we assessed their relationships with anatomical landmarks identifiable by microscopy or neurophysiological mapping, including the BG, insular gyri and sulcus, ventricular wall, and choroid plexus, using fused UHR-IA-CTA, MR tractography, and 3D-T1WI. 3D reconstructed or volume-rendered images were also used to facilitate anatomical interpretation (Supplementary Fig. 1C and 2). The anatomical relationships of the PT-LSAs to the Sylvian fissure and foramen of Monro were also examined to clarify PT-LSA localization according to the insular glioma classification proposed by Sanai and Berger [28]. To evaluate the anatomical relationship between the LSAs and tumor, images parallel to the PT-LSA course were generated.

Results

Patients

The demographic and clinical characteristics of the patients included in the anatomical analysis of the PT-LSAs are summarized in Table 1. Patient age ranged from 21 to 72 years (median, 46.5 years). The cohort included seven men and three women. Histological diagnoses were glioblastoma (n = 2), oligodendroglioma (n = 3), astrocytoma (n = 2), glioneuronal tumor (n = 1), and cortical dysplasia (n = 1). One patient had insular epilepsy without a histological abnormality.

Identification and anatomical characteristics of the PT-LSAs

The PT-LSAs were successfully identified in all 10 cases (Fig. 1 and Supplementary Fig. 3). One to four terminal PT-LSA branches were identified per patient (median, two branches) (yellow arrowheads in the Supplementary Fig. 1A). The overall course of the PT-LSAs was analyzed using the 3D-MIP images (Fig. 1 and Supplementary Fig. 3). The PT-LSAs were consistently located in the posterior and lateral portions of the LSA distribution on sagittal and coronal planes, respectively.

Anatomical relationship of the PT-LSAs to the PT and surrounding structures

3D reconstructions of the PT and BG showed that the PT courses along the posteromedial aspects of the putamen and the external and internal segments of the globus pallidus (Supplementary Fig. 2A). The PT-LSAs supplied the portion of the PT adjacent to the posteromedial putamen (Supplementary Fig. 2B).

In contrast, no PT-LSA supplied the portion of the PT medial to the external and internal segments of the globus pallidus.

To characterize the proximal course of the PT-LSA, we classified them according to their relationship with the insular central sulcus (ICS). PT-LSAs located posterior to the ICS were defined as posterior PT-LSAs, whereas those located beneath or anterior to the ICS were defined as anterior PT-LSA (Fig. 2). The anterior PT-LSAs coursed cranially and supplied the anterolateral and superior portions of the PT in six cases and the entire PT adjacent to the putamen in one case (red arrowheads in Figs. 1, 2, and 3 and Supplementary Fig. 3 and Table 1). The posterior PT-LSAs coursed posteriorly and cranially and supplied the posteromedial and inferior portions of the PT adjacent to the putamen in nine cases and the entire PT adjacent to the putamen in three cases (white arrowheads in Figs. 1, 2 and 3 and Supplementary Fig. 3, and Table 1).

The anterior PT-LSAs were located beneath the ICS in three cases and beneath the region extending from the anterior long gyri (ALG) through the ICS to the posterior short gyri (PSG) in the remaining three cases. After penetrating the putamen at its inferomedial aspect, the anterior PT-LSAs coursed laterally before changing direction superiorly and medially at the inferolateral aspects of the putamen, forming a characteristic bend termed the anterior curve (green arrowheads in Figs. 1 and 3 and Supplementary Fig. 3). Because the anterior curve represents the most lateral point of the anterior PT-LSA in the anteroposterior view, it serves as a useful anatomical landmark for predicting its course. The anterior curve was located beneath the ALG in three cases and beneath the ICS in three cases. Its depth from the insular surface ranged from 11 to 14 mm (mean ± standard deviation [SD], 12.2 ± 1.1 mm). Because dissection during resection of insular and temporal gliomas with insular infiltration is performed along the putaminal surface, the depth of the PT-LSA from the lateral putaminal surface is of particular surgical importance. The anterior PT-LSA coursed along the putaminal surface in five of six cases. The most lateral portion of the anterior curve and the more distal segment of the anterior PT-LSA were located on the putaminal surface in four and two cases, respectively (Fig. 3A and Table 2). The maximum and minimum depths from the putaminal surface ranged from 1 to 5 mm (mean ± SD, 2.6 ± 1.2 mm) and 0 to 3 mm (mean ± SD, 0.5 ± 1.1 mm), respectively (Table 2).

The posterior PT-LSAs were located beneath the ALG, postcentral insular sulcus, and posterior long gyri (PLG) in five, two, and two cases, respectively. At the posteroinferior aspect of the putamen, the putamen projects laterally and inferiorly, creating a depression immediately anterior to this projection (Fig. 3C). The posterior PT-LSA entered this depression from the medial or inferior side, coursed laterally and posteriorly, and then turned superiorly, medially, and posteriorly, forming a characteristic posterior curve in eight cases; the exception was Case 3 (blue arrowheads in Figs. 1 and 3 and Supplementary Fig. 3). Because the posterior curve represents the most posteroinferior point of the posterior PT-LSA in the lateral view, it serves as a useful anatomical landmark for predicting its course. The relationship of the posterior curve to the lateral ventricle and choroid plexus was also evaluated on fused volume-rendered LSA images from UHR-IA-CTA with 3D gadolinium-enhanced T1-weighted imaging (Gd-T1WI) (Fig. 3D). The posterior curve was located beneath the ALG in seven cases and beneath the PLG in two cases. Its

depth from the insular surface ranged from 8 to 14 mm (mean ± SD, 12.4 ± 1.9 mm). The posterior PT-LSA coursed along the putaminal surface in four of nine cases, either at the posterior curve (n = 2) (Fig. 3B) or in a more distal segment (n = 2) (Fig. 3D). The maximum and minimum depths from putaminal surface ranged from 1 to 6 mm (mean ± SD, 4.0 ± 1.3 mm) and 0 to 2 mm (mean ± SD, 0.8 ± 0.9 mm), respectively. The posterior curves were consistently located near the choroid plexus. Specifically, they were located 0–6 mm (mean ± SD, 2.0 ± 2.5 mm) anterior to the anterior end of the choroid plexus and 6–8 mm (mean ± SD, 6.6 ± 0.5 mm) superior to the roof of the lateral ventricle at the level of the anterior end of the choroid plexus (Fig. 3D) (Table 2).

These anatomical findings are summarized in Fig. 4.

According to the Sanai–Berger classification, all PT-LSAs were located within the deep portion of insular zone III and partially within zone II (Supplementary Fig. 4).

Intraoperative landmarks for localizing the PT-LSAs during glioma resection in their vicinity

We present a representative case illustrating the use of anatomical landmarks for intraoperative identification of the PT-LSAs (Fig. 5 and Supplementary Fig. 5).

A 44-year-old woman was referred to our hospital for recurrent isocitrate dehydrogenase (IDH)-mutant astrocytoma. The tumor was located in the right temporal lobe and extended into insular zone III (Fig. 5A). Both anterior and posterior PT-LSAs were identified (Supplementary Fig. 5A). The tumor closely infiltrated both PT-LSAs, which coursed within the putamen (Fig. 5B). The posterior PT-LSA curve was located 8 mm superior to the roof of the lateral ventricle at the level of the anterior end of the choroid plexus (Supplementary Fig. 5A) and beneath the junction of the ALG and PLG. The anterior PT-LSA was located beneath the ICS. Based on these findings, tumor resection was considered feasible by dissecting along the putaminal surface. Intraoperatively, the posterior PT-LSA was presumed to course within the putamen in an anterosuperior direction from the anterior end of the choroid plexus (Fig. 5C, bidirectional arrows in the upper left and lower panels), whereas the anterior PT-LSA was presumed to course within the putamen beneath the ICS, which runs parallel to the extension of the central sulcus (Fig. 5C, pink arrowheads in the upper left and right panels). The tumor was carefully dissected from the putamen anterior to the ICS (Fig. 5C, upper right panel). Subsequently, dissection was performed posteriorly along the putamen, with particular attention to the region beneath the ICS and anterosuperior to the anterior end of the choroid plexus (Fig. 5C, lower panel). Subtotal resection was achieved without postoperative neurological deficits attributable to ischemia resulting from PT-LSA injury (Supplementary Fig. 5B).

Discussion

In this study, we investigated the course of the PT-LSAs in patients with glioma or epilepsy without displacement of structures surrounding the LSAs using UHR-IA-CTA. Based on the course of their

proximal stems relative to the ICS, the PT-LSAs were classified as anterior or posterior branches. The PT-LSAs consistently coursed beneath the PSG, ICS, ALG, and PLG, within the deep portion of insular zone III, and along the lateral putaminal surface (Fig. 4). Consequently, these vessels are particularly vulnerable to injury during resection of temporal gliomas extending into the insula and insular gliomas involving zone III. Intraoperatively, the choroid plexus and ICS serve as reliable anatomical landmarks for localizing the PT-LSAs.

UHR-IA-CTA clearly showed the relationship between the terminal LSA branches and the PT (yellow arrowheads in Supplementary Fig. 1). Based on these high-resolution images, this study directly showed the anatomical relationships among the PT-LSA, PT, and BG, yielding three major findings. First, the PT-LSAs consistently supplied the PT coursing along the posteromedial aspect of the putamen. Considering that the putamen is primarily supplied by the LSAs [17] and that perforating arteries reach the PT after traversing the BG, this finding is anatomically consistent. Second, although LSA branching patterns are highly variable, as previously reported [1], we classified the proximal PT-LSA stems as anterior or posterior PT-LSAs according to their relationship with the ICS. The anterior and posterior PT-LSAs supplied the PT in 60% and 90% of cases, respectively. Their vascular territories were relatively consistent: the anterior PT-LSA supplied the anterolateral and superior portions of the PT adjacent to the putamen, whereas the posterior PT-LSA supplied the posteromedial and inferior portions. Although this characteristic anatomical course has been described in cadaveric studies [19, 20, 34], the present study is the first to directly show the corresponding perfusion territories within the PT. Third, the PT-LSAs consistently coursed through the deep portions of insular zones III and II according to the Sanai–Berger classification, which divides insular gliomas into four zones based on the Sylvian fissure and a perpendicular line passing through the foramen of Monro [28]. Resection of zone II insular gliomas is associated with lower resection rates because of the technical difficulty of surgical access and the close proximity to the PT [25, 28]. In contrast, zones III lesions, which are adjacent to the posterior temporal lobe, have generally been considered more amenable to resection [28]. However, Przybylowski et al. reported ischemic complications in 7 of 30 patients with zone III insular gliomas [25]. Although their study focused on differences in ischemic complications between transcortical and transsylvian approaches, these complications may also be attributable to the anatomical course of the PT-LSAs. Because zone III is frequently invaded by temporal gliomas, the present anatomical findings highlight the potential risk of PT-LSA injury during resection of both zone III insular gliomas and temporal gliomas extending into the insula.

Several intraoperative techniques, including indocyanine green video angiography [29] and power Doppler ultrasonography [32], have been described for identifying the LSAs. However, these methods require specialized equipment and have limited sensitivity for detecting the LSAs. Alternatively, several authors have proposed anatomical landmarks for intraoperative LSA localization. These include the LSA origin from the M1 segment of the MCA, the entry point into the anterior perforated substance [4, 24], and the uncinate fasciculus–inferior fronto-occipital fasciculus complex at the level of the limen insula [8, 9]. Furthermore, exposure of the beige-gray putaminal surface and lenticulostriate veins indicates that the dissection plane has approached the LSAs [24]. The present study further characterizes the

anatomical course of the PT-LSAs, including both anterior and posterior PT-LSAs, within the putamen and identifies regions of increased and reduced surgical risk. First, the anterior and posterior PT-LSAs frequently course along the lateral surface of the posterior putamen. Previous studies have indicated that the medial limit of insular glioma resection can be defined by the plane formed by the intraparenchymal course of the LSAs [4, 18]. However, distal PT-LSAs coursing along the putaminal surface are small and lack reliable depth landmarks, making them particularly susceptible to injury. To reduce this risk, the putamen should initially be exposed from its anterior aspect while avoiding dissection posterior to the ICS, which can be identified based on its relative position to the central sulcus. The dissection plane can subsequently be carefully extended into the region where the PT-LSAs course along the putaminal surface. Second, the PT-LSAs are particularly vulnerable at the anterior and posterior curves because these represent the most lateral and posteroinferior portions of their respective courses. These curves are closely associated with the anterior end of the choroid plexus and ICS, both of which are readily identifiable during surgery. Accordingly, these structures serve as reliable anatomical landmarks for estimating the PT-LSA course when putaminal distortion is minimal. A previous microdissection study similarly showed the close relationship between the anterior end of choroid plexus and the posterior curves of the LSAs supplying the posterior limb of the internal capsule [34]. We believe that this anatomical relationship remains clinically applicable even in gliomas causing putaminal distortion because internal decompression during tumor debulking typically reduces the distortion.

This study has several limitations that should be acknowledged. First, it did not evaluate the incidence of postoperative ischemic complications affecting the PT following surgical planning based on UHR-IA-CTA. Prospective studies focusing on surgical safety, extent of resection, and postoperative neurological outcomes are warranted to validate the clinical utility of this approach. Second, intraoperative localization of the LSAs supplying the PT-LSAs based on anatomical landmarks may require confirmation using intraoperative power Doppler ultrasonography or intraoperative MRI. Third, diffusion tensor imaging (DTI)-based tractography has inherent limitations, including susceptibility to crossing fibers and partial volume effects, which may reduce the accuracy of PT visualization. Correlating tractography findings with intraoperative observations, postoperative infarct distribution, and neurological outcomes may help further validate the anatomical relationships identified in this study.

Conclusion

The anatomical characteristics of the PT-LSAs were characterized using UHR-IA-CTA combined with multimodal imaging. Preoperative evaluation of the PT-LSAs provides valuable information for surgical planning. Intraoperatively, the ICS and choroid plexus serve as reliable anatomical landmarks for localizing the PT-LSAs during resection of insular gliomas and temporal gliomas extending into the insula and the putamen.

Declarations

Disclosures

Funding

The authors declare that no funding, grants, or other financial support were received for the preparation of this manuscript.

Conflict of Interests

The authors declare that they have no relevant financial or non-financial interests to disclose.

Ethics

This study was conducted in accordance with the Declaration of Helsinki, and approved by the Institutional Review Board of our hospital (2022-1-447).

Consent to participate and consent for publication

Written informed consent was obtained from all individual participants included in the study. This study contains no individual person's data.

Clinical trial number

Not applicable.

Submission guidelines

SRQR reporting guideline

Author contributions:

Conception and design: Masayuki Kanamori

Acquisition of data: Yuto Shingai, Masayuki Kanamori, Shin-Ichiro Osawa, Yoshiteru Shimoda, Kazuki Shimada, Kazutoshi Shirotori, Shingo Kayano, Shota Yamashita, Shunji Mugikura

Drafting the article: Yuto Shingai, Masayuki Kanamori

Critically revising the article: Shin-Ichiro Osawa, Shota Yamashita, Yoshiteru Shimoda, Shunji Mugikura

Reviewed submitted version of manuscript: all authors.

Study supervision: Hidenori Endo

References

1. Akashi T, Taoka T, Ochi T, Miyasaka T, Wada T, Sakamoto M, Takewa M, Kichikawa K (2012) Branching pattern of lenticulostriate arteries observed by MR angiography at 3.0 T. *Jpn J Radiol.* 2012;30(4):331–335. 10.1007/s11604-012-0058-7
2. Antoniello D, Ladsaria SS, Bhatia R (2025) Three-Dimensional Maps of the Lenticulostriate Artery Territory. Neurology 104(10):e213649. 10.1212/WNL.0000000000213649
3. Cho ZH, Kang CK, Han JY, Kim SH, Kim KN, Hong SM, Park CW, Kim YB (2008) Observation of the lenticulostriate arteries in the human brain in vivo using 7.0T MR angiography. Stroke 39(5):1604–1606. 10.1161/STROKEAHA.107.508002
4. Das KK, Rai S, Katyayan I, Madhesiya S, Srivastava AK, Jaiswal AK (2025) Microsurgical preservation of lenticulostriate artery perforators in insular glioma: the two point antegrade skeletonization technique. Acta Neurochir (Wien) 167(1):11. 10.1007/s00701-025-06422-w
5. Dasenbrock HH, See AP, Smalley RJ, Bi WL, Dolati P, Frerichs KU, Golby AJ, Chiocca EA, Aziz-Sultan MA (2019) Frameless Stereotactic Navigation during Insular Glioma Resection using Fusion of Three-Dimensional Rotational Angiography and Magnetic Resonance Imaging. World Neurosurg 126:322–330. 10.1016/j.wneu.2019.03.096
6. Djulejić V, Marinković S, Maliković A, Jovanović I, Djordjević D, Cetković M, Todorović V, Milisavljević M (2012) Morphometric analysis, region of supply and microanatomy of the lenticulostriate arteries and their clinical significance. J Clin Neurosci 19(10):1416–1421. 10.1016/j.jocn.2011.10.025
7. Djulejić V, Marinković S, Milić V, Georgievski B, Rašić M, Aksić M, Puškaš L (2015) Common features of the cerebral perforating arteries and their clinical significance. Acta Neurochir (Wien) 157(5):743–754 discussion 754. 10.1007/s00701-015-2378-8
8. Duffau H (2009) A personal consecutive series of surgically treated 51 cases of insular WHO Grade II glioma: advances and limitations. J Neurosurg 110(4):696–708. 10.3171/2008.8.JNS08741
9. Dziedzic TA, Bala A, Marchel A (2022) Anatomical aspects of the insula, opercula and peri-insular white matter for a transcortical approach to insular glioma resection. Neurosurg Rev 45(1):793–806. 10.1007/s10143-021-01602-5
10. Feekes JA, Hsu SW, Chaloupka JC, Cassell MD (2005) Tertiary microvascular territories define lacunar infarcts in the basal ganglia. Ann Neurol 58(1):18–30. 10.1002/ana.20505
11. Hervey-Jumper SL, Berger MS (2019) Insular glioma surgery: an evolution of thought and practice. J Neurosurg 130(1):9–16. 10.3171/2018.10.JNS181519
12. Horiuchi K, Suzuki K, Sasaki T, Matsumoto M, Sakuma J, Konno Y, Oinuma M, Itakura T, Kodama N (2005) Intraoperative monitoring of blood flow insufficiency during surgery of middle cerebral artery aneurysms. J Neurosurg 103(2):275–283. 10.3171/jns.2005.103.2.0275
13. Inoue G, Kanamori M, Osawa SI, Shimoda Y, Shimada K, Kayano S, Osada Y, Yamashita S, Mugikura S, Endo H (2025) Preoperative assessment of perforating arteries around amygdala glioblastoma using intra-arterial CT angiography with ultra-high-resolution CT and MR tractography: a case report. Acta Neurochir (Wien) 167(1):320. 10.1007/s00701-025-06741-y

14. Kang CK, Park CW, Han JY, Kim SH, Park CA, Kim KN, Hong SM, Kim YB, Lee KH, Cho ZH (2009) Imaging and analysis of lenticulostriate arteries using 7.0-Tesla magnetic resonance angiography. Magn Reson Med 61(1):136–144. 10.1002/mrm.21786
15. Kang HS, Han MH, Kwon BJ, Kwon OK, Kim SH, Chang KH (2005) Evaluation of the lenticulostriate arteries with rotational angiography and 3D reconstruction. AJNR Am J Neuroradiol 26(2):306–312
16. Kawaguchi T, Kumabe T, Saito R, Kanamori M, Iwasaki M, Yamashita Y, Sonoda Y, Tominaga T (2014) Practical surgical indicators to identify candidates for radical resection of insulo-opercular gliomas. J Neurosurg 121(5):1124–1132. 10.3171/2014.7.JNS13899
17. Kuzucu P, Çeltikçi P, Demirtaş OK, Canbolat Ç, Çeltikçi E, Demirci H, Özışık P, Tubbs RS, Pamir MN, Güngör A (2023) Arterial Supply of the Basal Ganglia: A Fiber Dissection Study. Oper Neurosurg 24(5):e351–e359. 10.1227/ons.0000000000000612
18. Lang FF, Olansen NE, DeMonte F, Gokaslan ZL, Holland EC, Kalhorn C, Sawaya R (2001) Surgical resection of intrinsic insular tumors: complication avoidance. J Neurosurg 95(4):638–650. 10.3171/jns.2001.95.4.0638
19. Marinkovic S, Gibo H, Milisavljevic M, Cetkovic M (2001) Anatomic and clinical correlations of the lenticulostriate arteries. Clin Anat 14(3):190–195. 10.1002/ca.1032
20. Marinkovic SV, Milisavljevic MM, Kovacevic MS, Stevic ZD (1985) Perforating branches of the middle cerebral artery. Microanatomy and clinical significance of their intracerebral segments. Stroke 16(6):1022–1029. 10.1161/01.str.16.6.1022
21. Murayama K, Suzuki S, Nagata H, Oda J, Nakahara I, Katada K, Fujii K, Toyama H (2020) Visualization of Lenticulostriate Arteries on CT Angiography Using Ultra-High-Resolution CT Compared with Conventional-Detector CT. AJNR Am J Neuroradiol 41(2):219–223. 10.3174/ajnr.A6377
22. Moshel YA, Marcus JD, Parker EC, Kelly PJ (2008) Resection of insular gliomas: the importance of lenticulostriate artery position. J Neurosurg 109(5):825–834. 10.3171/JNS/2008/109/11/0825
23. Osada Y, Kanamori M, Osawa SI, Kayano S, Uchida H, Shimoda Y, Mugikura S, Tominaga T, Endo H (2023) Visualization of the lenticulostriate arteries, long insular arteries, and long medullary arteries on intra-arterial computed tomography angiography with ultrahigh resolution in patients with glioma. Acta Neurochir (Wien) 165(12):4213–4219. 10.1007/s00701-023-05794-1
24. Pitskhelauri DI, Bykanov AE (2021) Complication avoidance: resection of the insular glioma complicated by iatrogenic injury to the lenticulostriate artery. Acta Neurochir (Wien) 163(11):3093–3096. 10.1007/s00701-021-04806-2
25. Przybylowski CJ, Baranoski JF, So VM, Wilson J, Sanai N (2019) Surgical morbidity of transsylvian versus transcortical approaches to insular gliomas. J Neurosurg 132(6):1731–1738. 10.3171/2018.12.JNS183075
26. Saito R, Kumabe T, Inoue T, Takada S, Yamashita Y, Kanamori M, Sonoda Y, Tominaga T (2009) Magnetic resonance imaging for preoperative identification of the lenticulostriate arteries in insular glioma surgery. Technical note. J Neurosurg 111(2):278–281. 10.3171/2008.11.JNS08858

27. Sakaji K, Shimoda Y, Kanamori M, Osawa SI, Yamashita S, Shimada K, Kayano S, Mugikura S, Endo H (2026) Preoperative visualization and intraoperative functional assessment of a long medullary artery in glioblastoma surgery using ultra-high-resolution intra-arterial Computed tomography angiography: an illustrative case. Br J Neurosurg 3:1–8. 10.1080/02688697.2026.2694473
28. Sanai N, Polley MY, Berger MS (2010) Insular glioma resection: assessment of patient morbidity, survival, and tumor progression. J Neurosurg 112(1):1–9. 10.3171/2009.6.JNS0952
29. Shah A, Rangarajan V, Kaswa A, Jain S, Goel A (2016) Indocyanine green as an adjunct for resection of insular gliomas. Asian J Neurosurg 11(3):276–281. 10.4103/1793-5482.175626
30. Shibahara I, Hanihara M, Miyasaka K, Sato S, Hide T, Kumabe T (2019) Temporal Glioblastoma Mimicking Basal Ganglia Invasion: Distinguishing Removable and Unremovable Tumors. World Neurosurg 130:e213–e221. 10.1016/j.wneu.2019.06.035
31. Sorimachi T, Osada T, Baba T, Inoue G, Atsumi H, Ishizaka H, Hotta K, Hayashi N, Matsumae M (2013) The striate artery, hematoma, and spot sign on coronal images of computed tomography angiography in putaminal intracerebral hemorrhage. Stroke 44(7):1830–1832. 10.1161/STROKEAHA.113.001498
32. Šteňo A, Jezberová M, Hollý V, Timárová G, Šteňo J (2016) Visualization of lenticulostriate arteries during insular low-grade glioma surgeries by navigated 3D ultrasound power Doppler: technical note. J Neurosurg 125(4):1016–1023. 10.3171/2015.10.JNS151907
33. Tatu L, Moulin T, Bogousslavsky J, Duvernoy H (1998) Arterial territories of the human brain: cerebral hemispheres. Neurology 50(6):1699–1708. 10.1212/wnl.50.6.1699
34. Ülkü G, Demirtaş OK, Lawton MT, Pamir MN, Güngör A (2024) Exploring arterial anatomy of the internal capsule: an analysis of the deep vascular structures and related white matter pathways. Neurosurg Rev 47(1):594. 10.1007/s10143-024-02781-7
35. Vogels V, Dammers R, van Bilsen M, Volovici V (2021) Deep Cerebral Perforators: Anatomical Distribution and Clinical Symptoms: An Overview. Stroke 52(10):e660–e674. 10.1161/STROKEAHA.120.034096

Tables

Table 1 and 2 are available in the Supplementary Files section.

Figures

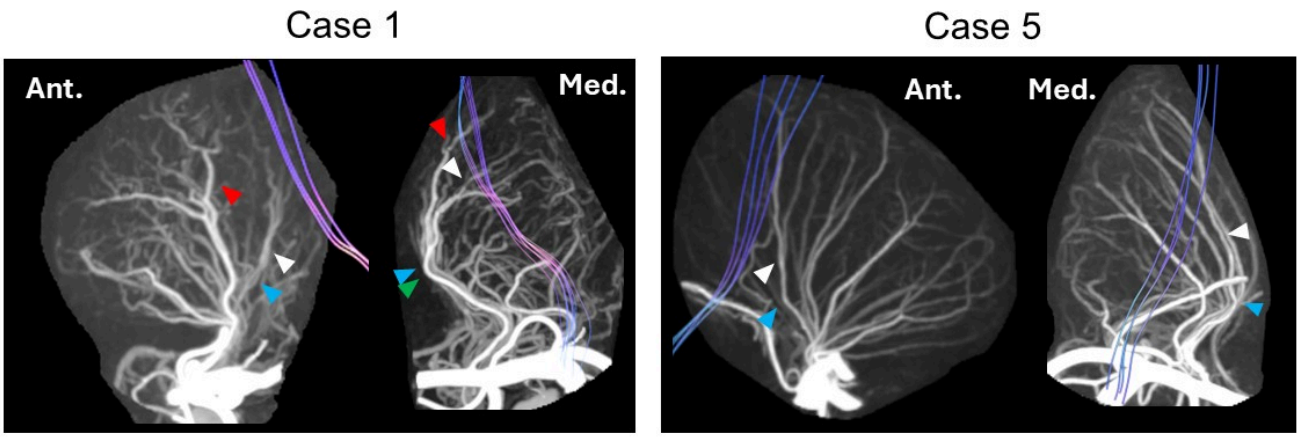


Figure 1

Representative three-dimensional maximum intensity projection images of the lenticulostriate arteries (LSAs) obtained by ultrahigh-resolution intra-arterial computed tomography angiography were fused with pyramidal tract (PT) fiber tracts in two patients with glioma without displacement of the LSA territory. (**A, B**) The left panels present lateral views (left-to-right for Case 1 and right-to-left for Case 5), and the right panels illustrate posterior views. The LSAs supplying the pyramidal tract (PT-LSAs) crossed the PT within the posterior-superior region of the fan-shaped LSA distribution. PT-LSAs located beneath or anterior to the insular central sulcus (ICS) were classified as anterior PT-LSAs (red arrowheads), whereas those located posterior to the ICS were classified as posterior PT-LSAs (white arrowheads). The anterior and posterior PT-LSAs supplies the PT in Case 1, whereas the posterior PT-LSA supplies the entire PT adjacent to the putamen in Case 5. The anterior and posterior PT-LSAs changed direction superiorly and medially at the anterior curve (blue arrowheads) and posterior curve (green arrowheads), respectively.

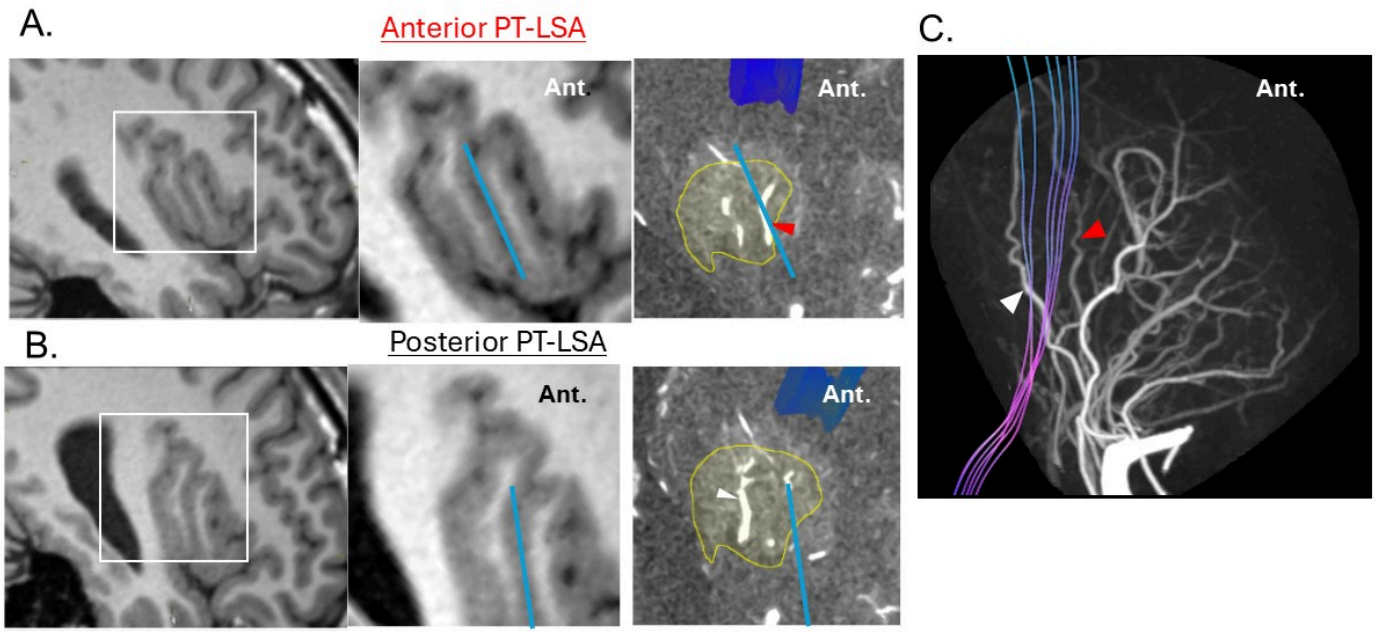


Figure 2

Classification of the lenticulostriate arteries supplying the pyramidal tract (PT-LSAs). (**A, B**) Relationship between the PT-LSAs and insular central sulcus (ICS). The left panels illustrate sagittal T1-weighted magnetic resonance imaging (MRI) of the insula (left panels), with enlarged views of the boxed regions in the adjacent panels highlighting the ICS (blue lines) (middle panels). On the corresponding synchronized sagittal ultrahigh-resolution intra-arterial computed tomography angiography images (right panels), the PT-LSAs beneath or anterior to the ICS (blue line) are defined as anterior PT-LSA (A), whereas those posterior to the ICS are defined as posterior PT-LSA (B). (**C**) Overview of the LSAs and PT on three-dimensional maximum intensity projection images obtained by ultrahigh-resolution intra-arterial computed tomography angiography fused with PT fiber tracts in Case 10. Red and white arrows denote the anterior and posterior PT-LSAs, respectively.

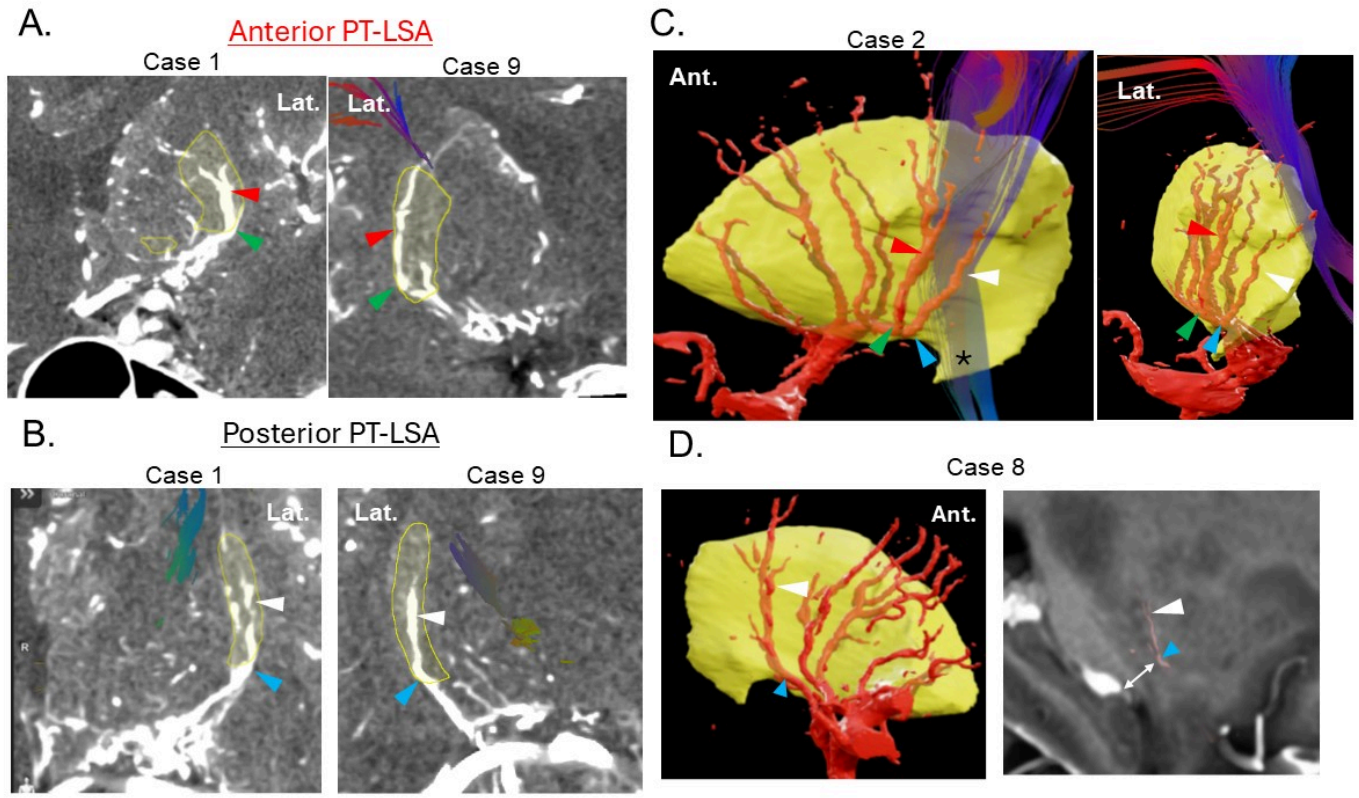


Figure 3

Relationship of the anterior and posterior lenticulostriate arteries supplying the pyramidal tract (PT-LSA) with the basal ganglia, PT, and choroid plexus. (**A**) Anterior view parallel to the anterior PT-LSA on ultrahigh-resolution intra-arterial computed tomography angiography (UHR-IA-CTA) fused with PT tractography and the automatically segmented putamen (yellow) from three-dimensional T1-weighted imaging (3D-T1WI). The anterior PT-LSA (red arrowhead) penetrated the inferomedial putamen, coursed laterally and superiorly, and changed direction at the anterior curve (green arrowheads). The anterior PT-LSA coursed along the putaminal surface only at the anterior curve in Case 1 and at both the anterior curve and its distal segment in Case 9. (**B**) Anterior view parallel to the posterior PT-LSA on UHR-IA-CTA fused with PT tractography and the automatically segmented putamen (yellow) from 3D-T1WI. The posterior PT-LSA penetrated the inferomedial putamen, coursed laterally and posteriorly, and then changed direction superiorly, medially, and posteriorly at the posterior curve (blue arrowheads). The posterior PT-LSA (white arrowheads) coursed along the putaminal surface at both the posterior curve and its distal segment in Case 1 and only at the posterior curve in Case 9. (**C**) Lateral (upper panel) and posterolateral (lower panel) 3D reconstructed images illustrating the relationships of the anterior PT-LSA (red arrowheads) and posterior PT-LSA (white arrowheads) with the putamen (yellow) and PT (blue streamlines). The asterisk denotes the posteroinferolateral projection of the putamen. The posterior PT-LSA entered the depression anterior to this projection from the medial or inferior side before coursing laterally and posteriorly. Both PT-LSAs changed direction at the inferior margin of the putamen. (**D**) Location of the posterior curve (blue arrowheads) of the posterior PT-LSA (white arrowhead) in Case 8. The left panel illustrates a lateral view of the 3D reconstructed image, and the right panel presents fused

volume-rendered LSA images from UHR-IA-CTA with gadolinium-enhanced 3D T1-weighted imaging. The bidirectional arrow denotes the distances from the roof of the lateral ventricle at the anterior end of the choroid plexus, and the posterior curve are indicated (bidirectional arrow).

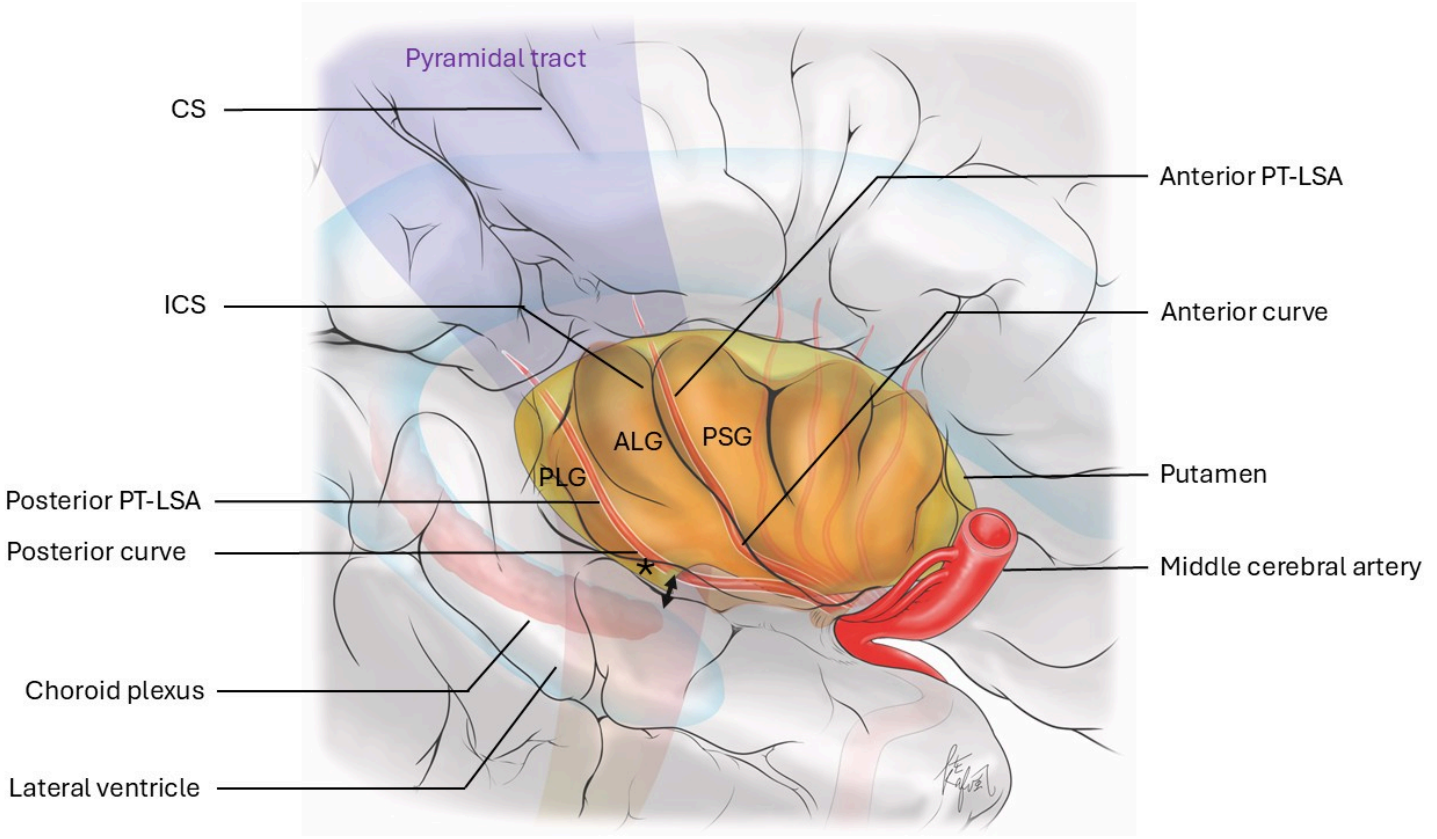


Figure 4

Schematic of the anatomical relationships among the right lenticulostriate arteries supplying the pyramidal tract (PT-LSAs), insula, choroid plexus, ventricle, and putamen. The anterior PT-LSAs were located beneath the insular central sulcus (ICS) or the region extending from the anterior long gyri (ALG) through the ICS to the posterior short gyri (PSG). The ICS runs parallel along the extension to the central sulcus.After coursing laterally, they changed direction superiorly and medially at the inferolateral putamen, forming the anterior curve, which was located beneath the ALG or ICS. The posterior PT-LSAs were located beneath the ALG, postcentral insular sulcus, or posterior long gyri (PLG). At the posteroinferior putamen, a posteroinferolateral projection (asterisk) creates a depression immediately anterior to it. The posterior PT-LSA entered this depression, coursed laterally and posteriorly, and then changed direction superiorly, medially, and posteriorly to form the posterior curve, which was located beneath the ALG or PLG. The posterior curve was situated close to the roof of the lateral ventricle at the level of the anterior end of the choroid plexus. The bidirectional arrow denotes the distance from the ventricular roof at the anterior end of the choroid plexus to the posterior curve.

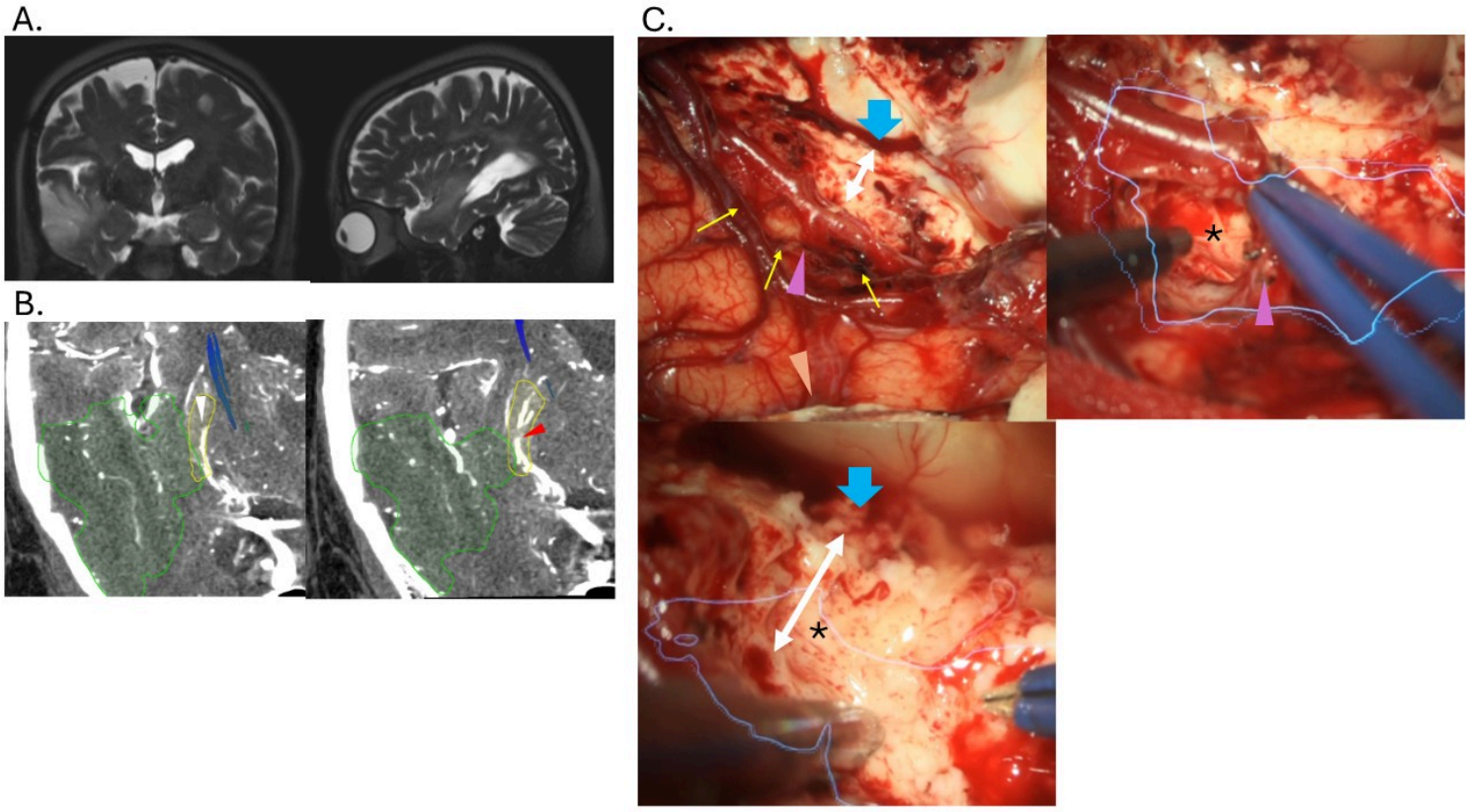


Figure 5

Representative case. A 44-year-old woman with recurrent isocitrate dehydrogenase-mutant astrocytoma. (**A**) Coronal and sagittal T2-weighted imaging (T2WI) showing a diffuse lesion in the right temporal lobe extending into insula zone III. (**B**) Preoperative images centered on the posterior (white arrowheads in the left panel) and anterior (red arrowheads in the right panel) PT-LSAs. These panels illustrate coronal images parallel to the PT-LSAs generated by fusing UHR-IA-CTA, 3D T1-weighted images (T1WI), and T2WI. The putamen (yellow) was automatically segmented on 3D T1WI, and the diffuse lesion (green) was manually segmented on 3D T2WI. The tumor closely infiltrated the posterior and anterior PT-LSAs, which coursed within the putamen. (**C**) Intraoperative findings. The insula (yellow arrows) and insular central sulcus (ICS; pink arrowheads), identified by the course of the M2 branches and the corresponding central sulcus (orange arrowhead) on the cerebral surface, were exposed (upper left panel). The tumor was carefully dissected from the putamen anterior to the ICS (upper right panel), and dissection was performed in a posterior direction along the putamen (asterisk) (upper right and lower panels). The locations of the posterior and anterior PT-LSA curves were estimated using the anterior end of the choroid plexus (blue arrow; upper left and lower panels) and ICS (upper left and upper right panels), respectively.

Supplementary Files

This is a list of supplementary files associated with this preprint. Click to download.

- FinalFileShingaietal.Table1..xlsx
- FinalFileShingaietal.Table2..xlsx
- FinalFileShingaietal.supplementaryfigures.docx